IEEE Access
Multidisciplinary : Rapid Review : Open Access Journal

Received May 3, 2020, accepted May 18, 2020, date of publication May 27, 2020, date of current version June 9, 2020.

Digital Object Identifier 10.1109/ACCESS.2020.2997989

Passivity-Based Control for Movable Multi-Load Inductively Coupled Power Transfer System Based on PCHD Model

XIN LI[1] AND XIANG LI[2]
[1]School of New Energy and Power Engineering, Lanzhou Jiaotong University, Lanzhou 730070, China
[2]School of Automation and Electrical Engineering, Lanzhou Jiaotong University, Lanzhou 730070, China

Corresponding authors: Xin Li (lixinzdh@lzjtu.edu.cn) and Xiang Li (lixiang13919170485@163.com)

This work was supported in part by the National Natural Science Foundation of China (project no.: 51767015), the Gansu Provincial Natural Science Foundation of China (Gansu Provincial Science and Technology Plan; project no.: 18JR3RA117) and Lanzhou Jiaotong University-Tianjin University Joint Innovation Fund Project (project no.: 2019051).

ABSTRACT A passivity-based control strategy for movable multi-load inductively coupled power transfer (ICPT) system based on PCHD (Port-Controlled Hamiltonian Dissipation, PCHD) model is proposed, which can effectively suppress mutual inductance and load interference. During the movement of the secondary coil of the movable multi-load ICPT system, due to the change of mutual inductance and the randomness of the multi-load, it will cause the transmission power and efficiency to oscillate and generate harmonics. Firstly, in view of the above problems, this paper analyzes the ICPT system under movable multiple loads. The DQ transformation method was used to establish the large-signal mathematical model of the system, and PCHD mathematical model in the DQ domain was established to decouple the active and reactive power. Secondly, the passivity-based controller (PBC) is designed by using the principle of interconnection and damping assignment passivity-based control (IDA-PBC). After that, the second method of Lyapunov function is used for stability analysis, and further verifies the asymptotic stability of the closed-loop system. Finally, the proposed method was verified by MATLAB/Simulink simulation. The simulation results show that the passivity-based controller has stronger robustness in both steady and movable states compared with the PI controller, which effectively suppresses the oscillation and total harmonic distortion caused by the change of mutual inductances and the randomness of the loads.

INDEX TERMS Movable multi-load ICPT system, PCHD model, IDA-PBC, passivity-based controller, PI controller, robustness.

I. INTRODUCTION

The movable multi-load ICPT system is a kind of power supply method based on the principle of electromagnetic induction. The power supply method uses long-rail coils or segmented coils to excite electrical energy on the primary side and uses multiple pickup coils to obtain electricity on the secondary side for high-power loads. It is widely used in dynamic power supply of high-power loads, such as dynamic wireless charging of multiple new energy electric vehicles, multiple movable manned sightseeing vehicles and contactless traction power supply of rail transit.

The associate editor coordinating the review of this manuscript and approving it for publication was Dazhong Ma.

However, due to the complex characteristics of ICPT system, e.g., high-order, nonlinear, uncertain, multimodal, autonomous oscillation, etc., [1], it is necessary to use appropriate control methods to ensure the system with high robust stability for power supply of high-power loads. In [2], a five-level high- frequency cascaded inverter is proposed to replace the traditional full-bridge inverter, which improved the system power by increasing the capacity of the inverter. At the same time, the influence of the system parameter perturbation on the stability of the system is also considered. According to the H_∞ and μ synthesis robust control method designed in [3]–[6], the multivariable tracking robust control without static error is realized, which restrained the frequency perturbation and loads change to a certain extent. In [7], an H_∞ controller is designed to deal with the problem of external

This work is licensed under a Creative Commons Attribution 4.0 License. For more information, see https://creativecommons.org/licenses/by/4.0/

disturbance and load uncertainty in the relay ICPT system. Since the misalignment of the coils in ICPT systems can result in fluctuation in power transmission or even instability of the ICPT systems, a μ-controller based on structured singular value (SSV) given in [8] is used to set up a closed-loop system to obtain robust control for ICPT system with coil misalignment.

Since the closed-loop control systems can obtain system stability and have good performance, the proportion and integration (PI) controllers are the most common ones used to establish closed-loop systems in industrial applications. In [9], a closed-loop PI controller system achieves good tracking performance without overshoot. However, for an ICPT system consisting of inverters, rectifiers, resonant and magnetic coupling units, is considered to be a system with high-order and nonlinearity, it is difficult to determine the parameter of the PI controllers. The PI controller needs to readjust the control parameters once the system parameters change and thus exhibited with poor stability and convergence performance, with an apparent overshoot. Moreover, the PI controller is not robust enough to eliminate the negative impact caused by parametric uncertainties,e.g., perturbation of the coupling coefficient k [6].

The above control methods have both advantages and disadvantages in terms of external disturbance, dynamic response, robustness against parameter changes, steady-state error and stability of the control circuit. The disadvantage is that all these methods do not consider the energy dissipation characteristics of the ICPT system. The energy dissipation properties play an important role in designing a control strategy for achieving global asymptotic stability, command tracking and strong robustness.

The passivity-based control (PBC) method is based on energy shaping and damping injection idea by using the energy dissipation properties of the system under certain considerations [10], [11]. The mathematical model of the PBC theory relies on the precise mathematical model of the research objects and the positive definite calculation of parameters to a great extent. This control strategy can effectively make up for a series of problems such as inaccurate parameter setting and poor robust stability in the PI controller [12]. Moreover, the interconnection and damping assignment passivity-based control (IDA-PBC) method allow designing high-performance nonlinear controllers for systems described by port-controlled Hamiltonian with dissipation models (PCHD) [13]. The Hamiltonian function represents, commonly, the physical system energy and can be regarded as the Lyapunov function. Given these advantages, the PBC method has recently attracted considerable attention in the field of electrical engineering [14]–[25].

Furthermore, the classical IDA-PBC method is proposed in [14]–[16] to ensure the regulation of inverters, it is illustrated that this method achieves satisfactory regulation performances. More specifically, PWM converter with LCL-filter [17] and multi paralleled VSCs with LCL filters [18], shunt active power filter [19] and type 2 STATCOM systems [20], AC/DC converters [21], distributed generation sources which are integrated to the power grid [22], the superconductor magnetic energy storage (SMES) [23], the mechanical systems [24] and electrical energy storage systems [25]. Although the PBC method has been successfully applied to the power electronics. For the sake of my knowledge, this metholodgy was not applied before to this ICPT systems. Therefore, it is important to study the PBC method of ICPT systems.

The significant contribution of this study is the possibility to suppress the oscillations of the transmission power and efficiency and the harmonics of the power in the ICPT system under the change of mutual inductance parameters and the randomness of the loads. Firstly, a second-order generalized integrator-quadrature signals generator (SOGI-QSG) can be used to construct the two-phase orthogonal vectors. Correspondingly, the large-signal mathematical models and PCHD models of the ICPT system are established. Secondly, according to the IDA-PBC method, the passivity-based controller of the ICPT system based on the PCHD model is designed. Then, the passive stability of the controller is analyzed according to the ''second method'' of Lyapunov. Finally, simulations implemented on MATLAB/Simulink are used to compare and analyze the performance of the passivity-based controller and the PI controller.

II. ANALYSIS OF THE WORKING PRINCIPLE OF MOVABLE MULTI-LOAD ICPT SYSTEM

The movable multi-load ICPT system is shown in Fig. 1. The DC voltage and current are U_{dc1}, U_{dc2} and i_{dc1}, i_{dc2}, respectively. u_1, i_1 is the fundamental wave components of the output voltage and current of the cascaded inverter, i_p and i_s are the currency of the primary and secondary coils, respectively. To ensure the system can sustain constant current on the primary side and constant voltage output on the secondary side, an LCL-S resonance compensation network can be selected once the load changes [26]. L_1, C_p and L_p constitute an LCL primary resonance compensation network, L_1 is the resonant inductance, C_p is the resonant compensation capacitor, L_p is the equivalent inductance of the transmitting coil. The equivalent inductance of the secondary pickup coils 1, 2 can be represented using L_{s1} and L_{s2}. M_1 and M_2 are mutual inductance of the coupling mechanism of the transmitting coil L_p and the pickup coils L_{s1} and L_{s2}. C_{s1}, C_{s2}, L_{s1} and L_{s2} composes an LC-type resonance network. M_s is the mutual inductance between the pickup coils L_{s1} and L_{s2}. R_{L1} and R_{L2} are equivalent resistance loads of the system, respectively. The cascaded inverter can invert the DC power into high-frequency AC power. After LCL resonance compensation, the high frequency alternating magnetic field will excite the high frequency alternating magnetic field in the transmitting coil L_p. According to the principle of electromagnetic induction, the load can obtain the same frequency of energy as the primary side.

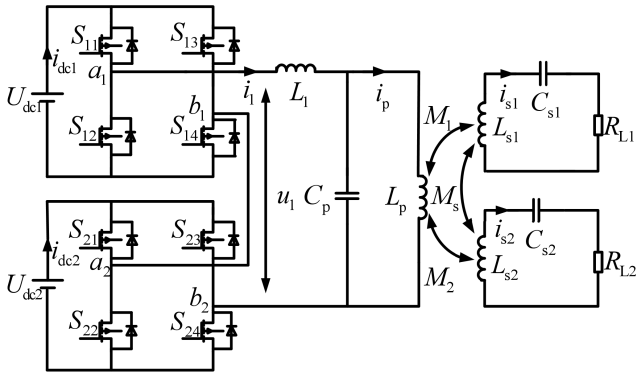

FIGURE 1. The circuit of movable multi-load ICPT system.

Once the ICPT system supplies power for loads, the switching state of the cascaded inverters in different ways will generate five different voltage levels, i.e., $2U_{dc}$, U_{dc}, 0, $-U_{dc}$ and $-2U_{dc}$. According to the switching state of the cascaded inverter, the binary logic switching functions of the left and right bridge arm can be set to S_{ia} and S_{ib} ($i = 1, 2$). Finally, the relationship between the values of U_{dci}, u_{1i}, i_{dci}, i_1 and the switch functions S_{ia} and S_{ib} is shown in Table 1.

TABLE 1. The logical relationship between the voltage, the current and the switching function.

S_{ia}	S_{ib}	i_{dci}	u_{1i}
0	0	0	0
0	1	-i_1	-U_{dci}
1	0	i_1	U_{dci}
1	1	0	0

As can be seen from Table 1, the functional relationship between the output level of the inverter and the switching state can be summarised into the following formula.

$$\begin{cases} u_1 = \sum_{i=1}^{2} (S_{ia} - S_{ib}) U_{dci} \\ i_{dci} = \sum_{i=1}^{2} (S_{ia} - S_{ib}) i_1 \end{cases} \tag{1}$$

The Fourier transform of the switching function S_{ik} (k = a, b, $i = 1, 2$) shown in the above formula (1) is obtained.

$$S_{ik} = d_{ik} + \sum_{n=1}^{\infty} (-1)^n \frac{2\sin(nd_{ik}\pi)\cos(n\omega_s t)}{n\pi} \tag{2}$$

where, d_{ik} is the mean value or duty cycle of the switching functions of the left and right bridge arms of the i-th unit, $\omega_s = 2\pi f_s$ is the angular frequency of the modulation wave.

The paper uses a high-frequency cascade inverter, which can be modulated by single-frequency carrier phase shift sinusoidal pulse width modulation (CPS-SPWM) [27]. Since the SPWM carrier frequency of the inverter is much higher than the frequency of the modulation wave, the harmonic term of S_{ik} in (2) can be omitted, so there is $S_{ik} \approx d_{ik}$. Then, the above formula (1) can be simplified as

$$\begin{cases} u_1 \approx (d_{ia} - d_{ib}) U_{dci} \\ i_{dci} \approx (d_{ia} - d_{ib}) i_1 \end{cases} \tag{3}$$

Ideally, let

$$\begin{cases} d_{ia} = \frac{1}{2} + \frac{m_i}{2}\sin(\omega_s t) \\ d_{ib} = \frac{1}{2} + \frac{m_i}{2}\sin(\omega_s t - 180°) \end{cases} \tag{4}$$

where, m_i is the modulation ratio ($m_i = 0.8$ [28]), which can satisfy $0 < m_i < 1$.

Finally, let the DC voltage be $U_{dc1} = U_{dc2} = U_{dc}$, the mathematical model of the five-level cascaded inverter can be obtained when combining the conditions that can satisfy (1), (2), (3) and (4), as shown in (5).

$$\begin{cases} u_1 = 2m_i U_{dc} \sin(\omega_s t) \\ i_{dc} = 2m_i i_1 \sin(\omega_s t) \end{cases} \tag{5}$$

III. MATHEMATICAL MODEL OF MOVABLE MULTI-LOAD ICPT SYSTEM

From the decoupled equivalent circuit of the LCL-S movable multi-load ICPT system given in Fig.2, the following assumptions can be made:

(1) The transmitting coil is a type of long straight track, and the magnetic field is evenly distributed.

(2) The distance between two pickup coils is very close, and the mutual inductance between them cannot be ignored, denoted as M_s.

(3) The internal resistance R_1, R_p, R_{s1}, R_{s2} of all coupling coils in the system should be considered comprehensively.

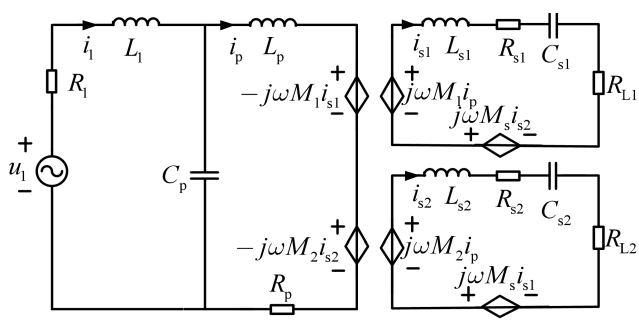

FIGURE 2. The decoupled equivalent circuit of the movable multi-load ICPT system.

The time domain equations of the system can be written in (6) with $d' = d/dt$ when taking the inductor current and capacitor voltage i_1, i_p, u_{Cp}, i_{s1}, i_{s2}, u_{Cs1}, u_{Cs2} of ICPT system as state variables according to the KCL and the KVL theorem.

$$\begin{cases} L_1 d' i_1 = -R_1 i_1 - u_{C_p} + u_1 \\ C_p d' u_{C_p} = i_1 - i_p \\ L_p d' i_p = -R_p i_p + j\omega M_1 i_{s1} + j\omega M_2 i_{s2} + u_{C_p} \\ L_{s1} d' i_{s1} = -(R_{s1} + R_{L1}) i_{s1} + j\omega M_s i_{s2} \\ \qquad\qquad + j\omega M_1 i_p - u_{C_{s1}} \\ L_{s2} d' i_{s2} = -(R_{s2} + R_{L2}) i_{s2} + j\omega M_s i_{s1} \\ \qquad\qquad + j\omega M_2 i_p - u_{C_{s2}} \\ C_{s1} d' u_{C_{s1}} = i_{s1} \\ C_{s2} d' u_{C_{s2}} = i_{s2} \end{cases} \tag{6}$$

where, $\omega = 2\pi f$ is the angular frequency of the excitation voltage of the system and f is the natural resonance frequency of each resonance link of the system. To ensure both the primary and the secondary side of the system work at the same resonant frequency to improve the power transmission capacity of the system, the ω should satisfy with

$$\omega = \frac{1}{\sqrt{L_{s1} C_{s1}}} = \frac{1}{\sqrt{L_{s2} C_{s2}}} = \frac{1}{\sqrt{L_p C_p}} \tag{7}$$

Once the system is in the state of constant current and voltage at both the primary and the secondary sides, the stability of the transmission power P and the coil transmission efficiency η of the system would be affected by the mutual inductance parameter M and the load R_L in the process of providing power to multiple loads.

The relationship curve between transmission power P and mutual inductances M_1 and M_2 is presented in Fig.3. From the figure, it is apparent that the transmission power of the system will increase or decrease nonlinearly when the mutual inductance parameter M_1 and M_2 of the system increase or decrease in the constant voltage output mode.

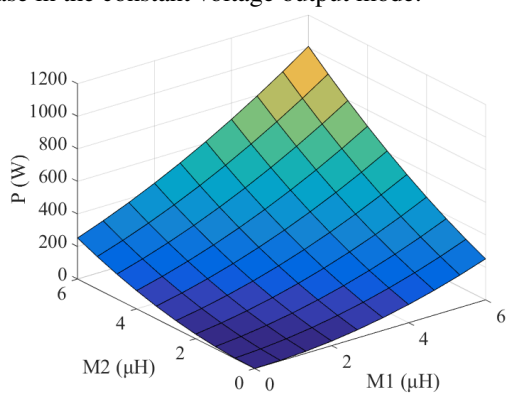

FIGURE 3. Relationship curve between transmission power P and mutual inductances M_1 and M_2.

The relationship between the transmission efficiency η and the loads R_{L1} and R_{L2} is given in Fig.4. When the load resistance increases, the transmission efficiency η of the system shows a downward trend. Among them, when the load resistance R_{L1} and R_{L2} value is very small, as the load resistance value increases, the transmission efficiency η drops greatly. When the load resistance value is large, the transmission efficiency decreases slowly. In the constant voltage output mode, the system can obtain a large transmission efficiency under heavy loads, while the transmission efficiency is low at light loads.

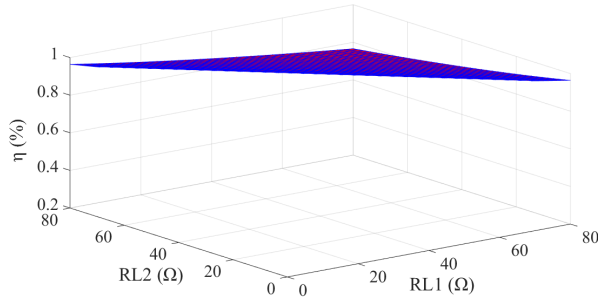

FIGURE 4. Relationship curve between transmission efficiency η and loads R_{L1} and R_{L2}.

Since the paper uses a single-phase cascaded inverter. It should be ensured that the inverter of the system has good signal filtering performance and fast response speed. A second-order generalized integrator-quadrature signals generator (SOGI-QSG) can be used to construct the two-phase orthogonal vectors [29]. The resonance frequency of the SOGI-QSG should be consistent with the operating resonance frequency of the ICPT system. The two-phase orthogonal vector constructed by SOGI-QSG is

$$\begin{cases} u_{1\alpha} = U_{1m} \cos(\omega t) \\ u_{1\beta} = U_{1m} \sin(\omega t) \\ i_{1\alpha} = I_{1m} \cos(\omega t - \varphi) \\ i_{1\beta} = I_{1m} \sin(\omega t - \varphi) \end{cases} \tag{8}$$

where, U_{1m}, I_{1m} is the output voltage and current peak of the inverter, $\varphi = 90°$ is the phase angles of the voltage leading current. It can be assumed that the voltage and current are $u_1 = u_\alpha$, $i_1 = i_\alpha$ in the α coordinate system. Then, the voltage and current components with the same imaginary amplitude and frequency and a phase difference of 90° can be obtained in the β coordinate system. Hence, the components of the single-phase AC signal in the two-phase stationary $\alpha\beta$ coordinate system are $u_{1\beta}$, i_β, respectively. Finally, the AC component in the $\alpha\beta$ stationary coordinate system can be converted into the DC component in the DQ rotating coordinate system [30]. The equivalent rotation coordinate transformation formula of the system is.

$$\begin{cases} \begin{bmatrix} u_{1d} \\ u_{1q} \end{bmatrix} = \begin{bmatrix} \cos(\omega t) & \sin(\omega t) \\ -\sin(\omega t) & \cos(\omega t) \end{bmatrix} \begin{bmatrix} u_{1\alpha} \\ u_{1\beta} \end{bmatrix} \\ \begin{bmatrix} i_{1d} \\ i_{1q} \end{bmatrix} = \begin{bmatrix} \cos(\omega t) & \sin(\omega t) \\ -\sin(\omega t) & \cos(\omega t) \end{bmatrix} \begin{bmatrix} i_{1\alpha} \\ i_{1\beta} \end{bmatrix} \end{cases} \tag{9}$$

Substituting the above formula (9) into the time domain differential equation of the system shown in (6). The system's state variables i_1, i_p, u_{Cp}, i_{s1}, i_{s2}, u_{Cs1}, u_{Cs2} can be converted into DC components on the DQ coordinate with the sine and the cosine components of each equation are separated. Then, the large-signal model of ICPT system can be obtained, as is shown in bellow.

$$\begin{cases} L_1 d' i_{1d} = -R_1 i_{1d} + \omega L_1 i_{1q} - u_{C_{pd}} + u_{1d} \\ L_1 d' i_{1q} = -\omega L_1 i_{1d} - R_1 i_{1q} - u_{C_{pq}} + u_{1q} \\ C_p d' u_{C_{pd}} = i_{1d} - i_{pd} + \omega C_p u_{C_{pq}} \\ C_p d' u_{C_{pq}} = i_{1q} - i_{pq} - \omega C_p u_{C_{pd}} \\ L_p d' i_{pd} = u_{C_{pd}} - R_p i_{pd} + \omega L_p i_{pq} \\ \qquad - \omega M_1 i_{s1q} - \omega M_2 i_{s2q} \\ L_p d' i_{pq} = u_{C_{pq}} - R_p i_{pq} - \omega L_p i_{pd} \\ \qquad + \omega M_1 i_{s1d} + \omega M_2 i_{s2d} \\ L_{s1} d' i_{s1d} = -\omega M_1 i_{pq} - (R_{s1} + R_{L1}) i_{s1d} \\ \qquad + \omega L_{s1} i_{s1q} - \omega M_s i_{s2q} - u_{C_{s1d}} \\ L_{s1} d' i_{s1q} = \omega M_1 i_{pd} - \omega L_{s1} i_{s1d} \\ \qquad - (R_{s1} + R_{L1}) i_{s1q} + \omega M_s i_{s2d} - u_{C_{s1q}} \\ L_{s2} d' i_{s2d} = -\omega M_2 i_{pq} - \omega M_s i_{s1q} \\ \qquad - (R_{s2} + R_{L2}) i_{s2d} + \omega L_{s2} i_{s2q} - u_{C_{s2d}} \\ L_{s2} d' i_{s2q} = \omega M_2 i_{pd} + \omega M_s i_{s1d} - \omega L_{s2} i_{s2d} \\ \qquad - (R_{s2} + R_{L2}) i_{s2q} - u_{C_{s2q}} \\ C_{s1} d' u_{C_{s1d}} = i_{s1d} + \omega C_{s1} u_{C_{s1q}} \\ C_{s1} d' u_{C_{s1q}} = i_{s1q} - \omega C_{s1} u_{C_{s1d}} \\ C_{s2} d' u_{C_{s2d}} = i_{s2d} + \omega C_{s2} u_{C_{s2q}} \\ C_{s2} d' u_{C_{s2q}} = i_{s2q} - \omega C_{s2} u_{C_{s2d}} \end{cases} \tag{10}$$

where, i_{1d}, i_{1q}, u_{Cpd}, u_{Cpq}, i_{pd}, i_{pq}, i_{s1d}, i_{s1q}, i_{s2d}, i_{s2q}, u_{Cs1d}, u_{Cs1q}, u_{Cs2d}, u_{Cs2q} are the DC component of state variables i_1, i_p, u_{Cp}, i_{s1}, i_{s2}, u_{Cs1}, u_{Cs2} in the DQ coordinate system.

IV. DESIGN OF PASSIVITY-BASED CONTROLLER FOR ICPT SYSTEM

A. THE PCHD MODEL OF MOVABLE MULTI-LOAD ICPT SYSTEM

The general form of the Port-controlled Hamiltonian with Dissipation (PCHD) model is

$$\begin{cases} \dot{x} = [J(x) - R(x)]\dfrac{\partial H(x)}{\partial x} + g(x)u \\ y = g^{\mathrm{T}}(x)\dfrac{\partial H(x)}{\partial x} \end{cases} \tag{11}$$

where, x is the state variable matrix, u is the control variable matrix, y is the output variable, $J(x)$ is the interconnection matrix with antisymmetric characteristics, $R(x)$ is the dissipation matrix with symmetric and positive definite, $g(x)$ is a structural matrix that reflects the direct effect of system control variables on state variables, $H(x)$ is the energy storage function of the system.

Select the inductor flux and capacitor charge of the ICPT system as state variables:

$$\begin{aligned} x &= [x_1\ x_2\ x_3\ x_4\ x_5\ x_6\ x_7\ x_8\ x_9\ x_{10}\ x_{11}\ x_{12}\ x_{13}\ x_{14}]^{\mathrm{T}} \\ &= [L_1 i_{1d}\ L_1 i_{1q}\ C_p u_{C_{pd}} \\ &\qquad C_p u_{C_{pq}}\ L_p i_{pd}\ L_p i_{pq}\ L_{s1} i_{s1d}\ L_{s1} i_{s1q}\ L_{s2} i_{s2d}\ L_{s2} i_{s2q} \\ &\qquad C_{s1} u_{C_{s1d}}\ C_{s1} u_{C_{s1q}}\ C_{s2} u_{C_{s2d}}\ C_{s2} u_{C_{s2q}}]^{\mathrm{T}} \end{aligned}$$

Set the (Hamiltonian) energy storage function of the ICPT system:

$$\begin{aligned} H(x) &= \left(x_1^2 + x_2^2\right)/2L_1 + \left(x_3^2 + x_4^2\right)/2C_p + \left(x_5^2 + x_6^2\right)/2L_p \\ &\quad + \left(x_7^2 + x_8^2\right)/2L_{s1} + \left(x_9^2 + x_{10}^2\right)/2L_{s2} \\ &\quad + \left(x_{11}^2 + x_{12}^2\right)/2C_{s1} + \left(x_{13}^2 + x_{14}^2\right)/2C_{s2} \\ &= \frac{1}{2} x^{\mathrm{T}} D x \end{aligned} \tag{12}$$

where,

$$D = \mathrm{diag}\begin{Bmatrix} 1/L_1 & 1/L_1 & 1/C_p & 1/C_p & 1/L_p & 1/L_p & 1/L_{s1} \\ 1/L_{s1} & 1/L_{s2} & 1/L_{s2} & 1/C_{s1} & 1/C_{s1} & 1/C_{s2} & 1/C_{s2} \end{Bmatrix}$$

The PCHD model of the system can be obtained by combining the mathematical model of the system shown in the above equations (10) with the equations (11), where $J(x)$, $g(x)$, $R(x)$, $\frac{\partial H(x)}{\partial x}$ and u, as shown at the bottom of the next page.

B. PASSIVE ANALYSIS OF MOVABLE MULTI-LOAD ICPT SYSTEM

If the PBC strategy is used in the single-phase ICPT system, it must be guaranteed that the system is considered to be strictly passive. Therefore, before designing the passivity-based controller for the single-phase system, the passivity of the system should be analyzed. For general systems, if there are a semi-definite and continuously differentiable energy storage function $H(x)$ and a positive definite function $Q(x)$. For $\forall\, t > 0$, the dissipation inequality can satisfy

$$\begin{cases} H(x(t)) - H(x(0)) \le \int_0^t u^{\mathrm{T}} y d\tau - \int_0^t Q(x) d\tau \\ \dot{H}(x) \le u^{\mathrm{T}} y - Q(x) \end{cases} \tag{13}$$

where $x(t)$, $u(t)$, and $y(t)$ represent the state, input, and output vectors, respectively. $H(x(t)) - H(x(0))$ represents the energy stored inside the ICPT system, and $u^{\mathrm{T}} y$ represents the external energy supplied to the ICPT system. $Q(x)$ represents the dissipated energy in the system. Since the dissipated energy always propels the state $x(t)$ back to the desired equilibrium point, the passive system is inherently stable. That is, as long as the system is passive, it must be internally stable. The detailed proof of strict passivity for the ICPT system is given mathematically below. Based on (10), the power balance equation is listed as follows:

$$\begin{aligned} & L_1 i_{1d} d' i_{1d} + L_1 i_{1q} d' i_{1q} + C_p u_{C_{pd}} d' u_{C_{pd}} + C_p u_{C_{pq}} d' u_{C_{pq}} \\ &\quad + L_p i_{pd} d' i_{pd} + L_p i_{pq} d' i_{pq} + L_{s1} i_{s1d} d' i_{s1d} + L_{s1} i_{s1q} d' i_{s1q} \\ &\quad + L_{s2} i_{s2d} d' i_{s2d} + L_{s2} i_{s2q} d' i_{s2q} + C_{s1} u_{C_{s1d}} d' u_{C_{s1d}} \\ &\quad + C_{s1} u_{C_{s1q}} d' u_{C_{s1q}} + C_{s2} u_{C_{s2d}} d' u_{C_{s2d}} + C_{s2} u_{C_{s2q}} d' u_{C_{s2q}} \\ &= u_{1d} i_{1d} + u_{1q} i_{1q} - [R_1(i_{1d}^2 + i_{1q}^2) + R_p(i_{pd}^2 + i_{pq}^2) \\ &\quad + (R_{s1} + R_{L1})(i_{s1d}^2 + i_{s1q}^2) + (R_{s2} + R_{L2})(i_{s2d}^2 + i_{s2q}^2)] \end{aligned} \tag{14}$$

which can be further simplified to

$$\begin{aligned} & d'[L_1 i_{1d}^2/2 + L_1 i_{1q}^2/2 + C_p u_{C_{pd}}^2/2 + C_p u_{C_{pq}}^2/2 + L_p i_{pd}^2/2 \\ &\quad + L_p i_{pq}^2/2 + L_{s1} i_{s1d}^2/2 + L_{s1} i_{s1q}^2/2 + L_{s2} i_{s2d}^2/2 + L_{s2} i_{s2q}^2/2 \\ &\quad + C_{s1} u_{C_{s1d}}^2/2 + C_{s1} u_{C_{s1q}}^2/2 + C_{s2} u_{C_{s2d}}^2/2 + C_{s2} u_{C_{s2q}}^2/2] \end{aligned}$$

$$= u_{1d}i_{1d} + u_{1q}i_{1q} - [R_1(i_{1d}^2 + i_{1q}^2) + R_p(i_{pd}^2 + i_{pq}^2) + (R_{s1} + R_{L1})(i_{s1d}^2 + i_{s1q}^2) + (R_{s2} + R_{L2})(i_{s2d}^2 + i_{s2q}^2)]$$

We set

$$\begin{aligned} H(x) = {} & [L_1 i_{1d}^2/2 + L_1 i_{1q}^2/2 + C_p u_{C_{pd}}^2/2 + C_p u_{C_{pq}}^2/2 \\ & + L_p i_{pd}^2/2 + L_p i_{pq}^2/2 + L_{s1} i_{s1d}^2/2 + L_{s1} i_{s1q}^2/2 \\ & + L_{s2} i_{s2d}^2/2 \\ & + L_{s2} i_{s2q}^2/2 + C_{s1} u_{C_{s1d}}^2/2 + C_{s1} u_{C_{s1q}}^2/2 + C_{s2} u_{C_{s2d}}^2/2 \\ & + C_{s2} u_{C_{s2q}}^2/2] = \left(x^T D x\right)/2 > 0 \\ u^T y = {} & u_{1d}i_{1d} + u_{1q}i_{1q} \\ Q(x) = {} & [R_1(i_{1d}^2 + i_{1q}^2) + R_p(i_{pd}^2 + i_{pq}^2) + (R_{s1} + R_{L1})(i_{s1d}^2 + i_{s1q}^2) \\ & + (R_{s2} + R_{L2})(i_{s2d}^2 + i_{s2q}^2)] > 0. \end{aligned}$$

From the above formulas, it can be found that the energy of the ICPT system satisfies (13). Thus, the movable multi-load ICPT system is strictly passive and the PBC strategy can be used in the ICPT system.

C. DESIGN OF PASSIVITY-BASED CONTROLLER FOR ICPT SYSTEM BASED ON IDA-PBC

According to the IDA-PBC theorem, for a known passive system, the $J(x)$, $R(x)$, $H(x)$, $g(x)$ and the expected stable equilibrium point $x^* \in R^n$ are all determined. Suppose we can find the functions u, $J_a(x)$, $R_a(x)$ and vector functions $K(x) = \partial H_a(x)/\partial x$ satisfy

$$[J(x) - R(x)]\frac{\partial H(x)}{\partial x} + g(x)u = [J_d(x) - R_d(x)]\frac{\partial H_d(x)}{\partial x} \tag{15}$$

the following conditions are true:

(1) Conservation of structure

$$\begin{cases} J_d(x) = J(x) + J_a(x) = -J_d^T(x) \\ R_d(x) = R(x) + R_a(x) = R_d^T(x) \geq 0 \\ H_d(x) = H(x) + H_a(x) \end{cases} \tag{16}$$

(2)Integrability, the vector function $K(x)$ satisfies

$$\partial K(x)/\partial x = (\partial K(x)/\partial x)^T \tag{17}$$

$$J(x) = \begin{bmatrix} 0 & \omega L_1 & -1 & 0 & 0 & 0 & 0 & 0 & 0 & 0 & 0 & 0 & 0 & 0 \\ -\omega L_1 & 0 & 0 & -1 & 0 & 0 & 0 & 0 & 0 & 0 & 0 & 0 & 0 & 0 \\ 1 & 0 & 0 & \omega C_p & -1 & 0 & 0 & 0 & 0 & 0 & 0 & 0 & 0 & 0 \\ 0 & 1 & -\omega C_p & 0 & 0 & -1 & 0 & 0 & 0 & 0 & 0 & 0 & 0 & 0 \\ 0 & 0 & 1 & 0 & 0 & \omega L_p & 0 & -\omega M_1 & 0 & -\omega M_2 & 0 & 0 & 0 & 0 \\ 0 & 0 & 0 & 1 & -\omega L_p & 0 & \omega M_1 & 0 & \omega M_2 & 0 & 0 & 0 & 0 & 0 \\ 0 & 0 & 0 & 0 & 0 & -\omega M_1 & 0 & \omega L_{s1} & 0 & -\omega M_s & -1 & 0 & 0 & 0 \\ 0 & 0 & 0 & 0 & \omega M_1 & 0 & -\omega L_{s1} & 0 & \omega M_s & 0 & 0 & -1 & 0 & 0 \\ 0 & 0 & 0 & 0 & 0 & -\omega M_2 & 0 & -\omega M_s & 0 & \omega L_{s2} & 0 & 0 & -1 & 0 \\ 0 & 0 & 0 & 0 & \omega M_2 & 0 & \omega M_s & 0 & -\omega L_{s2} & 0 & 0 & 0 & 0 & -1 \\ 0 & 0 & 0 & 0 & 0 & 0 & 1 & 0 & 0 & 0 & 0 & \omega C_{s1} & 0 & 0 \\ 0 & 0 & 0 & 0 & 0 & 0 & 0 & 1 & 0 & 0 & -\omega C_{s1} & 0 & 0 & 0 \\ 0 & 0 & 0 & 0 & 0 & 0 & 0 & 0 & 1 & 0 & 0 & 0 & 0 & \omega C_{s2} \\ 0 & 0 & 0 & 0 & 0 & 0 & 0 & 0 & 0 & 1 & 0 & 0 & -\omega C_{s2} & 0 \end{bmatrix}$$

$$g(x) = \begin{bmatrix} 1 & 0 & 0 & 0 & 0 & 0 & 0 & 0 & 0 & 0 & 0 & 0 & 0 & 0 \\ 0 & 1 & 0 & 0 & 0 & 0 & 0 & 0 & 0 & 0 & 0 & 0 & 0 & 0 \\ 0 & 0 & 0 & 0 & 0 & 0 & 0 & 0 & 0 & 0 & 0 & 0 & 0 & 0 \\ 0 & 0 & 0 & 0 & 0 & 0 & 0 & 0 & 0 & 0 & 0 & 0 & 0 & 0 \\ 0 & 0 & 0 & 0 & 0 & 0 & 0 & 0 & 0 & 0 & 0 & 0 & 0 & 0 \\ 0 & 0 & 0 & 0 & 0 & 0 & 0 & 0 & 0 & 0 & 0 & 0 & 0 & 0 \\ 0 & 0 & 0 & 0 & 0 & 0 & 0 & 0 & 0 & 0 & 0 & 0 & 0 & 0 \\ 0 & 0 & 0 & 0 & 0 & 0 & 0 & 0 & 0 & 0 & 0 & 0 & 0 & 0 \\ 0 & 0 & 0 & 0 & 0 & 0 & 0 & 0 & 0 & 0 & 0 & 0 & 0 & 0 \\ 0 & 0 & 0 & 0 & 0 & 0 & 0 & 0 & 0 & 0 & 0 & 0 & 0 & 0 \\ 0 & 0 & 0 & 0 & 0 & 0 & 0 & 0 & 0 & 0 & 0 & 0 & 0 & 0 \\ 0 & 0 & 0 & 0 & 0 & 0 & 0 & 0 & 0 & 0 & 0 & 0 & 0 & 0 \\ 0 & 0 & 0 & 0 & 0 & 0 & 0 & 0 & 0 & 0 & 0 & 0 & 0 & 0 \\ 0 & 0 & 0 & 0 & 0 & 0 & 0 & 0 & 0 & 0 & 0 & 0 & 0 & 0 \end{bmatrix}$$

$$R(x) = \mathrm{diag}(R_1, R_1, 0, 0, R_p, R_p, R_{s1} + R_{L1}, R_{s1} + R_{L1}, R_{s2} + R_{L2}, R_{s2} + R_{L2}, 0, 0, 0, 0);$$

$$\frac{\partial H(x)}{\partial x} = [i_{1d}\ i_{1q}\ u_{C_{pd}}\ u_{C_{pq}}\ i_{pd}\ i_{pq}\ i_{s1d}\ i_{s1q}\ i_{s2d}\ i_{s2q}\ u_{C_{s1d}}\ u_{C_{s1q}}\ u_{C_{s2d}}\ u_{C_{s2q}}]^T;$$

$$u = \left[u_{1d}\ u_{1q}\ 0\ 0\ 0\ 0\ 0\ 0\ 0\ 0\ 0\ 0\ 0\right]^T.$$

(3) $H_d(x)$ has an extreme value at x^*. The existence of extreme values at x^* requires the vector function $K(x)$ to satisfy

$$K(x^*) = -(\partial H(x)/\partial x)|_{x=x^*} \tag{18}$$

(4) $H_d(x)$ has a minimum at x^*.then at this point of x^*, according to the Lyapunov stability, the Jacobian matrix of $K(x)$ should satisfy

$$\frac{\partial K(x)}{\partial x}|_{x=x^*} + \frac{\partial^2 H(x)}{\partial x^2}|_{x=x^*} = \frac{\partial^2 H_d(x)}{\partial x^2}|_{x=x^*} > 0 \tag{19}$$

Under these conditions, the PCHD closed-loop model of the system is shown below

$$\dot{x} = [J_d(x) - R_d(x)]\frac{\partial H_d(x)}{\partial x} \tag{20}$$

where, $J_d(x)$ and $R_d(x)$ are the new interconnection matrix and dissipation matrix respectively; $R_a(x)$ is the damping injection matrix, which is a positive definite matrix; $H_a(x)$ is a pending function, which means the energy injected into the system through control; $H_d(x)$ is the total energy storage function, and satisfies x^* =argmin$H_d(x)$, the expected equilibrium state x^* is the state of the smallest $H_d(x)$ point of the total energy storage function.

Substituting $J_d(x)$, $R_d(x)$, $K(x)$ and $H_a(x)$ into equation (15), the PBC can be obtained:

$$u = g^{-1}(x)\left([J_d(x) - R_d(x)]\frac{\partial H_d(x)}{\partial x} - [J(x) - R(x)]\frac{\partial H(x)}{\partial x}\right) \tag{21}$$

Due to the following conditions:

$$\begin{cases} \partial H(x)/\partial x = Dx \\ \partial H_d(x)/\partial x = Dx_e \\ \partial H_a(x)/\partial x = \partial H_d(x)/\partial x - \partial H(x)/\partial x = -Dx^* \end{cases} \tag{22}$$

Substituting the condition of equation (22) into equation (21), the passivity-based controller is

$$u = g^{-1}(x)[J_a(x) - R_a(x)]Dx - g^{-1}(x)[J_d(x) - R_d(x)]Dx^* \tag{23}$$

It can be known from the PBC shown in equation (23) that the controller is determined by J_a, R_a, and $K(x)$. From the literature [31], we can know that J_a, R_a and $K(x)$ can take different values or functions, and usually $J_a = 0$, $R_a = 0$ or $K(x)$ is a simple function. When $J_a = 0$ and $R_a = 0$, the convergence rate of the system is uncontrollable, the performance of the system is negative. When $J_a = 0$, $R_a \neq 0$, that is, when the damping R_a is injected, the system can obtain good control performance. Therefore, it is necessary to comprehensively consider the influence of energy shaping and damping injection on the control performance of the system. We can choose $J_a = 0$ and $R_a \neq 0$ schemes [32], [33]. The desired equilibrium point of the system can be confirmed and the error variable is $x_e = x - x^*$. The expected energy storage function of ICPT system is

$$H_d(x) = \frac{1}{2}x_e^T D x_e = \frac{1}{2}(x - x^*)^T D(x - x^*) \tag{24}$$

Let the desired equilibrium point of the system be

$$\begin{aligned} x^* &= [x_1^* \; x_2^* \; x_3^* \; x_4^* \; x_5^* \; x_6^* \; x_7^* \; x_8^* \; x_9^* \; x_{10}^* \; x_{11}^* \; x_{12}^* \; x_{13}^* \; x_{14}^*]^T \\ &= [L_1 i_{1d}^* \; L_1 i_{1q}^* \; C_p u_{C_{pd}}^* \; C_p u_{C_{pq}}^* \; L_p i_{pd}^* \\ &\quad L_p i_{pq}^* \; L_{s1} i_{s1d}^* \; L_{s1} i_{s1q}^* \; L_{s2} i_{s2d}^* \\ &\quad L_{s2} i_{s2q}^* \; C_{s1} u_{C_{s1d}}^* \; C_{s1} u_{C_{s1q}}^* \; C_{s2} u_{C_{s2d}}^* \; C_{s2} u_{C_{s2q}}^*]^T \end{aligned}$$

Let the pending interconnection and damping injection matrix be

$$\begin{cases} J_a(x) = 0 \\ R_a(x) = \mathrm{diag}(r_1, r_2, r_3, r_4, r_5, r_6, r_7, r_8, r_9, \\ r_{10}, r_{11}, r_{12}, r_{13}, r_{14}) \\ R_d(x) = \mathrm{diag}\,(R_1 + r_1, R_1 + r_2, r_3, r_4, R_p + r_5, R_p + r_6, \\ R_{s1} + R_{L1} + r_7, R_{s1} + R_{L1} + r_8, R_{s2} + R_{L2} + r_9, \\ R_{s2} + R_{L2} + r_{10}, r_{11}, r_{12}, r_{13}, r_{14}) \end{cases}$$

The above formulas (21), (22) and (23) can be combined and simplified to obtain the passivity-based controller. As shown in equation (25).

$$u = -[J(x) - R_d(x)]Dx^* - R_a(x)Dx \tag{25}$$

Substituting the interconnection matrix and injection damping into the large-signal model shown in equation (10), As shown in equation (26), a large-signal model with switching signals u_{1d}, u_{1q} can be obtained.

$$\begin{cases} u_{1d} + r_1 i_{1d} = (R_1 + r_1)i_{1d}^* - \omega L_1 i_{1q}^* + u_{C_{pd}}^* \\ u_{1q} + r_2 i_{1q} = \omega L_1 i_{1d}^* + (R_1 + r_2)i_{1q}^* + u_{C_{pq}}^* \end{cases} \tag{26}$$

Substituting the formula (26) into the PBC shown in (25), the control rate of the passivity-based controller of the ICPT system can be obtained.

$$\begin{cases} u_{1d} = (R_1 + r_1)i_{1d}^* - r_1 i_{1d} - \omega L_1 i_{1q}^* + u_{C_{pd}}^* \\ u_{1q} = \omega L_1 i_{1d}^* + (R_1 + r_2)i_{1q}^* - r_2 i_{1q} + u_{C_{pq}}^* \end{cases} \tag{27}$$

where, r_1 and r_2 are injection damping of the ICPT system. It follows from (24) that $x \to x^*$ based on the Lyapunov stability criterion, which means that the control objective is achieved with the PBC (27). Substituting the control rate of the system shown in equation (27) into the first two equations of the large-signal model shown in equation (10), the dynamic model of the system can be obtained as shown in equation (28) below.

$$\begin{cases} L_1 d' i_{1d} = (R_1 + r_1)(i_{1d}^* - i_{1d}) + \omega L_1(i_{1q} - i_{1q}^*) \\ \qquad + (U_{C_{pd}}^* - U_{C_{pd}}) \\ L_1 d' i_{1q} = (R_1 + r_2)(i_{1q}^* - i_{1q}) + \omega L_1(i_{1d}^* - i_{1d}) \\ \qquad + (U_{C_{pq}}^* - U_{C_{pq}}) \end{cases} \tag{28}$$

From equation (28), the injection of the damping r_1 and r_2 will accelerate the convergence of the system in the dynamic

process. The speed of $H_d(x) \rightarrow 0$ is mainly on r_1 and r_2, which principally determines the robustness of the ICPT system to system parameter changes and external disturbances. Ignoring the strong coupling of the system, the variable $L_1 i_{1d}$, $L_1 i_{1q}$, $C_P U_{Cpd}$ and $C_P U_{Cpq}$ converges to the desired equilibrium point $L_1 i_{1d}^*$, $L_1 i_{1q}^*$, $C_P U_{Cpd}^*$ and $C_P U_{Cpq}^*$.

According to the passivity-based controller rate shown in equation (27), the passivity-based controller of the system can be obtained, as shown in Fig. 5.

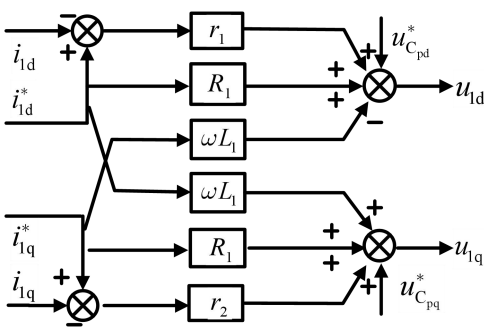

FIGURE 5. Schematic diagram of the passivity-based controller.

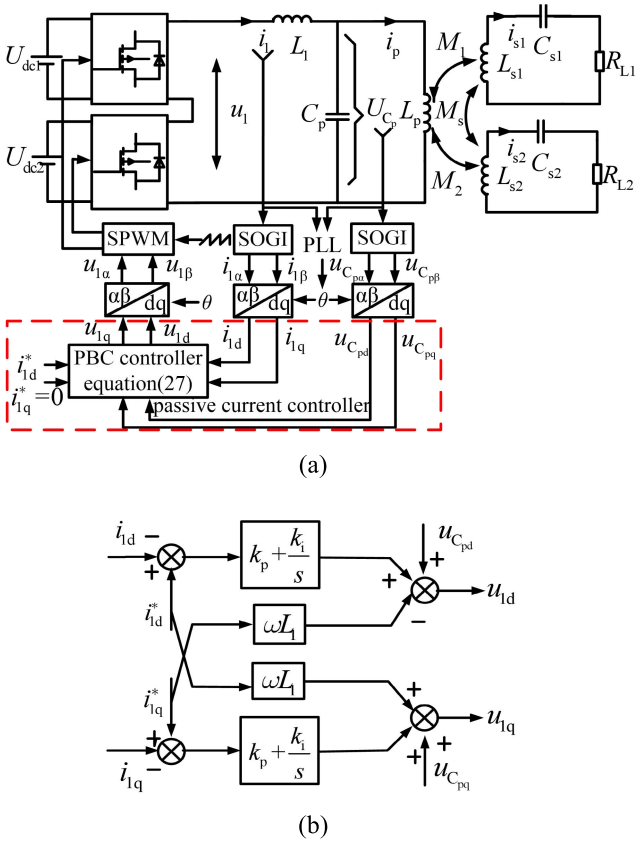

FIGURE 6. The whole control block diagram of the ICPT system. (a) The passivity-based controller scheme of the movable multi-load ICPT system; (b) The PI controller.

Since the cascaded inverter is modulated by CPS-SPWM in this paper. The switching signals u_{1d}, u_{1q} of the PBC control rate need to be converted into the input signals $u_{1\alpha}$, $u_{1\beta}$ of the CPS-SPWM modulation module. The switching signal shown in the above formula (27) can be substituted into the inverse Park transform formula shown in (29)

$$\begin{bmatrix} u_{1\alpha} \\ u_{1\beta} \end{bmatrix} = \begin{bmatrix} \cos(\omega t) & -\sin(\omega t) \\ \sin(\omega t) & \cos(\omega t) \end{bmatrix} \begin{bmatrix} u_{1d} \\ u_{1q} \end{bmatrix} \tag{29}$$

Fig. 6 (a) and (b) shows proposed PBC scheme and the classical d-q PI current linear controller scheme [34]. In this paper, the SOGI-QSG is used to construct a two-phase quadrature vector and a phase-locked loop (PLL) [35] is used to lock the phase θ for the DQ transform. It provides a high-performance detection system, which can accurately characterize the extracted variables even in the state of system internal parameter perturbation and external interference.

D. PASSIVE STABILITY ANALYSIS OF ICPT SYSTEM

Compared with the guardian map theory based on Kronecker sum proposed by [36], the Second Method of Lyapunov is used to verify the global stability of the passivity-based controller in this paper. Considering the $H_d(x)$ is a positive definite function that is equal to zero only at the equilibrium point, it can be directly selected as a Lyapunov function for stability analysis. Since the stability of ICPT system depends on the first derivative of $H_d(x)$, it can be obtained that the first derivative of $H_d(x)$ is

$$\begin{aligned} \dot{H}\mathrm{d}(x) &= \frac{\partial H_d^T(x)}{\partial x}\dot{x} = \frac{\partial H_d^T(x)}{\partial x}[J_d(x) - R_d(x)]\frac{\partial H_d(x)}{\partial x} \\ &= -\frac{\partial H_d^T(x)}{\partial x}R_d(x)\frac{\partial H_d(x)}{\partial x} \end{aligned} \tag{30}$$

It can be known from(15)

$$\begin{cases} J_d(x) = -J_d^T(x) \Rightarrow [\partial H_d^T(x)]/\partial x] J_d(x)[\partial H_d(x)/\partial x] = 0 \\ R_d(x) = R_d^T(x) \geq 0 \end{cases} \tag{31}$$

Hence, when substituting equation (31) into equation (30), the above equation can be simplified as

$$\dot{H}_d(x) = -\left(\partial H_d^T(x)/\partial x\right) R_d(x)\,(\partial H_d(x)/\partial x) \leq 0 \tag{32}$$

From formula (32), the convergence rate of $H_d(x)$ is mainly determined by R_a. Here, $H_d(x)$ can be used as a Lyapunov function and no solution $x(t)$ can stay in the set except x^*

$$\left\{ x \in R^n \,\middle|\, \left(\partial^T H_d(x)/\partial x\right) R_d(x)\,(\partial H_d(x)/\partial x) = 0 \right\} \tag{33}$$

Among them, La Salle's invariant set theorem shows that x^* is the equilibrium point of the asymptotic stability of the system. Besides, the difference with the injection damping r_a in [34], [35] is the difference in the control rate of the Euler-Lagrange (EL) model and PCHD model. The injection damping r_1 and r_2 in this paper are self-setting constants. Compared with the method in [37], the mathematical model is established by using the DQ coordinate system in this paper, which can realize the decoupling of active power and reactive power. The error and the error storage function can make the

controller easier to design and the dynamic performance of the ICPT system is also improved. However, the injection damping in [37] is zero, which can also speed up the system to stable.

V. SIMULATION TESTS AND ANALYSIS

To verify the efficiency of the PBC method proposed in this paper. The MATLAB/ Simulink is utilized to compare and verify the efficiency of the passivity-based controller and the PI controller. The injection damping of the ICPT system can be selected as $r_1 = 4\Omega$ and $r_2 = 4\Omega$. The specific stimulation parameter settings of the system are shown in Table 2.

TABLE 2. Simulation parameters.

Symbol	Parameters of PBC and PI	Value
U_{dc1}, U_{dc2}	DC power supply	300V，300V
f	Inverter frequency	25kHz
L_1, R_1	Primary resonance coil inductance and internal resistance	60μH, 0.001Ω
C_p	The primary resonance compensation capacitor	40μF
L_p, R_p	Transmitting coil inductance and internal resistance	1.0μH, 0.001Ω
L_{s1}, L_{s2}	Pickup coil inductance	206.4μH, 230.7μH
M_1, M_2	Mutual inductance of launch and pickup coils	3.04μH, 3.00μH
M_s	Mutual inductance between pickup coils	3.56μH
C_{s1}, C_{s2}	Pickup circuit compensation capacitor	0.19μF, 0.17μF
R_{s1}, R_{s2}	Pickup coil internal resistance	0.001Ω，0.001Ω
R_{L1}, R_{L2}	Load Resistance	30Ω，30Ω

This paper uses SOGI-QSG with the same structure to extract two-phase voltages $U_{Cp\alpha}$, $U_{Cp\beta}$ and currents i_α, i_β. The resonance frequency of the signal is the same as the frequency of SOGI-QSG. Therefore, the extracted voltage and current have the same Bode diagram and transfer function. The stability and convergence of the two-phase signal are only related to the change of k value. The control structure of the SOGI-QSG is shown in Fig. 7 below.

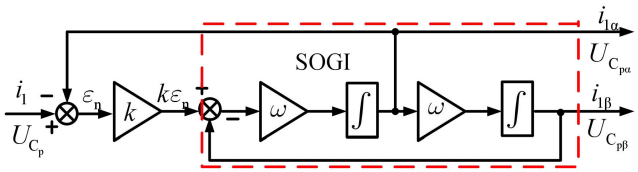

FIGURE 7. The control structure of the SOGI-QSG.

The transfer function of the second-order generalized integrator (SOGI) is

$$\begin{cases} f_{SOGI}(s) = \dfrac{i_{1\alpha}(s)}{k\varepsilon_n(s)} = \dfrac{\omega s}{s^2+\omega^2} \\ f_{SOGI}(s) = \dfrac{U_{C_{p\alpha}}(s)}{k\varepsilon_n(s)} = \dfrac{\omega s}{s^2+\omega^2} \end{cases} \tag{34}$$

Compared with the existing literature regarding closed-loop transfer function methods [38]. The closed-loop transfer function of SOGI-QSG is directly derived from the control structure and precise parameters of the system. It can ensure accuracy and convergence and stability has been significantly improved. The closed-loop transfer function of the SOGI-QSG can be obtained:

$$\begin{cases} H_{i_{1\alpha}}(s) = \dfrac{i_{1\alpha}(s)}{i_1(s)} = \dfrac{k\omega s}{s^2+k\omega s+\omega^2} \\ H_{i_{1\beta}}(s) = \dfrac{i_{1\beta}(s)}{i_1(s)} = \dfrac{k\omega^2}{s^2+k\omega s+\omega^2} \\ H_{U_{C_{p\alpha}}}(s) = \dfrac{U_{C_{p\alpha}}(s)}{U_{C_p}(s)} = \dfrac{k\omega^2}{s^2+k\omega s+\omega^2} \\ H_{U_{C_{p\beta}}}(s) = \dfrac{U_{C_{p\beta}}(s)}{U_{C_p}(s)} = \dfrac{k\omega^2}{s^2+k\omega s+\omega^2} \end{cases} \tag{35}$$

where, ω is the resonance frequency of SOGI; ε_n is the phase angle error signal; k is the gain.

According to the closed-loop transfer function shown in the above formula (35), given the value of k is changed, the Bode diagram of SOGI is shown in Fig.8.

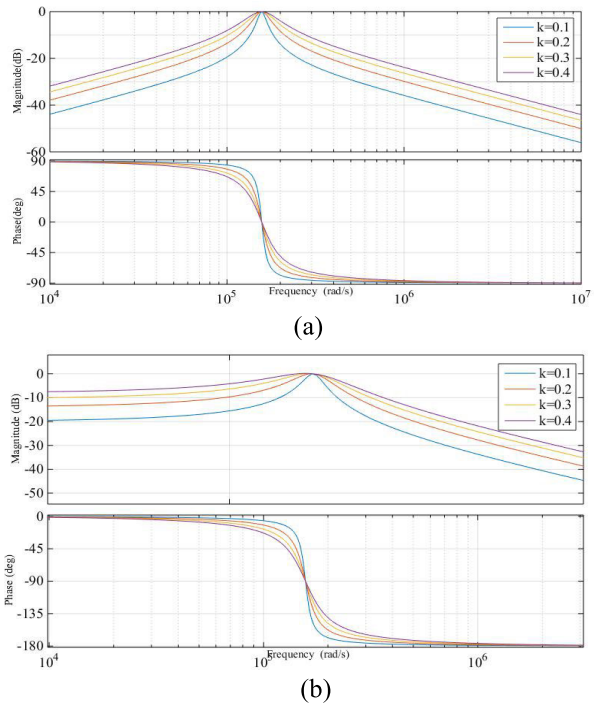

FIGURE 8. The bode diagram of the SOGI. (a) The bode diagram of the $H_{i\alpha}$ (s) and $H_{UCP\alpha}$ (s); (b) The bode diagram of the $H_{i\beta}$ (s) and $H_{UCP\beta}$(s).

Fig.8 (a) and (b) shows the phase difference between H_α(s) and H_β(s) is 90°. The phase difference does not change with the change of the gain k. When the system is running at the inverter frequency ω, the two-phase fundamental signals have the same amplitude and phase characteristics, namely i_α(s)= i_β(s) and $U_{Cp\alpha}$(s)= $U_{Cp\beta}$(s). It will not be affected by changes in k. However, The change of gain k will affect the stability, response speed and filtering performance of the extracted signals. Therefore, the value of k needs to be adjusted reasonably to resolve the contradiction between response speed and filtering delay.

By comparing and analyzing the performance of the two-phase signals under different gain k. The best empirical k can be obtained to confirm the stability of the signal and improve the response speed. Through a comprehensive analysis and comparative study of the effect of different k values on the stability of the signal, it is finally determined that $k = 0.1$ is the optimal value.

Fig.9(a) shows the output voltage and current simulation waveform of the cascaded inverter. From the simulation waveforms, the output voltage of the cascade inverter is five levels and the voltage and current waveforms are stable. It is also beneficial to use the SOGI to extract a stable two-phase fundamental signal. The superiority of the control performance of the designed controller is ensured. Fig. 9 (b) and (c) show the simulation waveform of the two-phase fundamental signal. From the simulation waveform, the two-phase fundamental wave signal $U_{\mathrm{Cp}\alpha}$, $U_{\mathrm{Cp}\beta}$ and i_α, i_β have a stable sinusoidal waveform and the response speed of the waveform is fast and the filtering is strong.

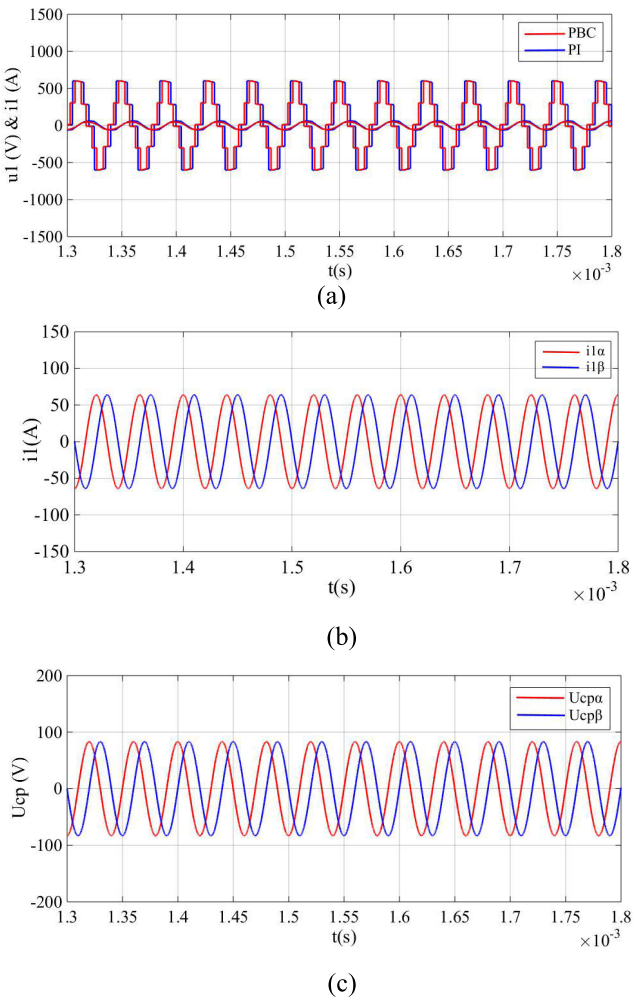

FIGURE 9. Simulation waveform. (a) The voltage and current simulation waveform of the cascaded inverter; (b) Current waveform; (c) Voltage waveform.

The two-phase AC voltage $U_{\mathrm{Cp}\alpha}$, $U_{\mathrm{Cp}\beta}$ and current i_α, i_β can be converted to U_{Cpd}, U_{Cpq}, and $i_{1\mathrm{d}}$, $i_{1\mathrm{q}}$ by Park transformation. Fig. 10 (a) and(b) shows the response curve of DC voltage U_{Cpd}, U_{Cpq} and current $i_{1\mathrm{d}}$, $i_{1\mathrm{q}}$. From the response curve, after the reference state variable is given, the passivity-based controller can track the given reference value more quickly and it can keep the reactive voltage and current at 0. The response curve shows that the proposed PBC strategy has better steady-state performance and faster dynamic response. Fig. 10 (c) shows the sine fundamental wave signal U_α and U_β response curve. After the PBC control, the fundamental wave signals $U_{1\alpha}$ and $U_{1\beta}$ after reverse Park transformation can be obtained. The signal has a stable sinusoidal waveform. It can be compared with a phase-shifted triangular carrier to generate an SPWM modulation signal, which acted on the cascaded inverter.

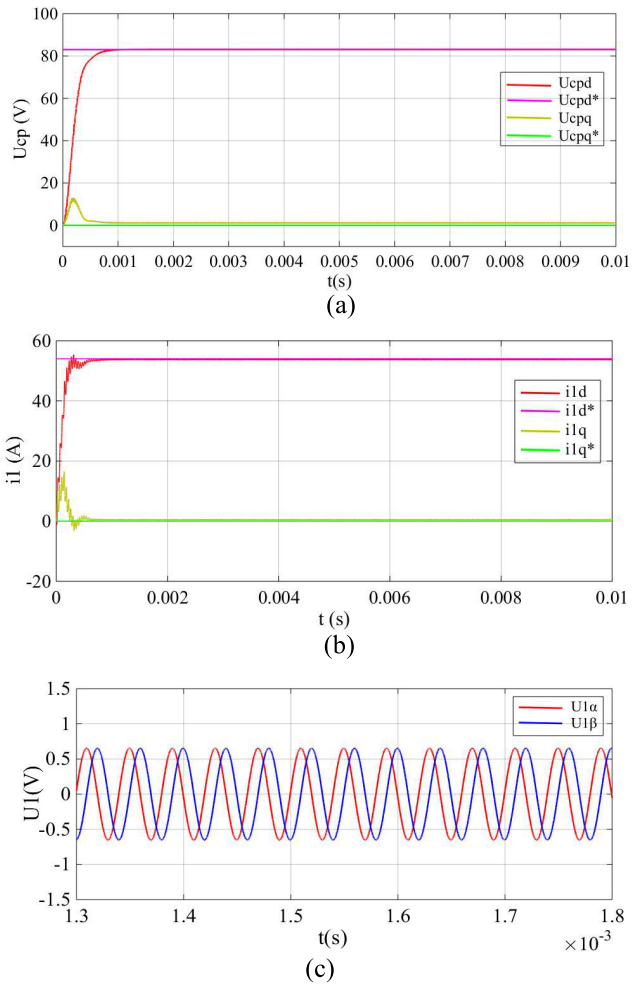

FIGURE 10. Simulation waveform. (a) The response curve of voltage U_{Cpd}, U_{Cpq}; (b) The response curve of current i_{1d}, i_{1q}; (c) Sine fundamental wave signal $U_{1\alpha}$, $U_{1\beta}$.

Fig. 11 shows the voltage and current waveform diagram of the primary coil of the system. There are some differences in

the simulation waveforms. From the simulation waveforms, with the designed passivity-based controller, the voltage and current waveforms on the primary side of the system quickly reach a stable-state and have rapid convergence. However, due to an apparent overshoot of the PI controller, the voltage and current waveforms fluctuate before reaching a steady-state quickly.

According to the Fast Fourier Transform (FFT), the frequency spectrum of the primary voltage and current is analyzed. The total harmonic distortion (THD) of the primary voltage and current is shown in Table 3 below. Available from Table, the THD of the U_p is decreased from 0.47% to 0.23% and the THD of the i_p is reduced from 0.17% to 0.10%.

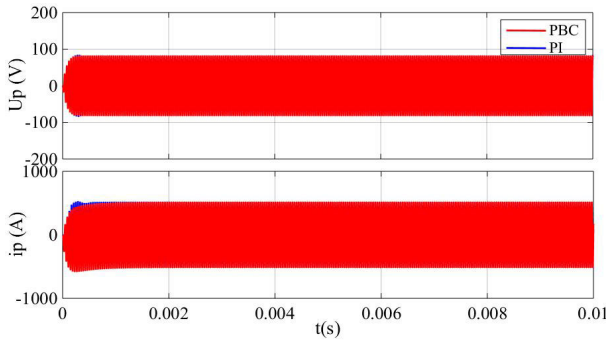

FIGURE 11. Simulation result of the primary side.

TABLE 3. The THD of the primary voltage and current.

Control method	THD% of the U_p(V)	THD% of the i_p(A)
PBC	0.23	0.10
PI	0.47	0.17

According to the principle of electromagnetic induction, the secondary side pickup coil will receive power from the primary coil. Fig. 12 (a) and (b) shows the simulation waveform diagram of the secondary voltage and current. From the simulation waveforms, similarly, with the designed PBC, the voltage and current waveform of the secondary voltage of the system quickly reach a stable state, and have rapid convergence. However, due to the appearance of the PI controller, the voltage and current waveforms also fluctuate before reaching a steady-state quickly. It can be seen that the steady-state performance of the PI controller is worse than that of the PBC, and the convergence of the PI controller shows much worse performance, with an apparent overshoot.

The total harmonic distortion (THD) of the secondary voltage and current is shown in Table 4 below. Available from Table, the THD of the U_s was reduced from 0.23% to 0.12% and the THD of the i_s was decreased from 0.17% to 0.10%.

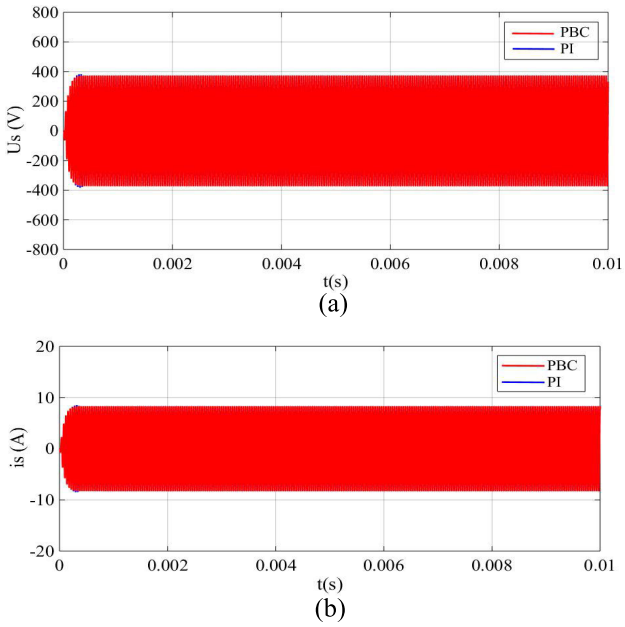

FIGURE 12. Simulation waveform of the secondary side. (a) The voltage waveform ofthe secondary side; (b) The current waveform ofthe secondary side.

TABLE 4. The THD of the secondary voltage and current.

Control method	THD% of the U_s(V)	THD% of the i_s(A)
PBC	0.12	0.10
PI	0.23	0.17

Fig. 13 (a) and (b) shows the waveform diagram of the voltage and current obtained by the loads. From the simulation, with the designed PBC, the load voltage and current of the system reach a stable-state in a short time, with rapid convergence. However, because the PI controller has a significant overshoot characteristic, the voltage and current waveforms of the load fluctuate equally before reaching a steady-state. The the total harmonic distortion (THD) of the loads voltage and current is shown in Table 5 below. From the Table, the total harmonic distortion (THD) of the load voltage was reduced from 0.15% to 0.06% and the THD of the load current was decreased from 0.17% to 0.08%. The passivity-based controller is found to reduce the total harmonic distortion (THD) of the ICPT system.

Fig. 14(a) shows a comparison of the active power response performance between the PI controller and the PBC. Since the designed PBC is also applicable to the control of the active power, the active power response curve quickly reaches a steady-state in a short time. However, the designed PI controller makes the active power response curve fluctuate up and down before reaching a steady-state. Therefore, the steady-state performance of the PI controller is worse than the passivity-based controller. Before reaching the steady-state, the PI controller has a significant overshoot.

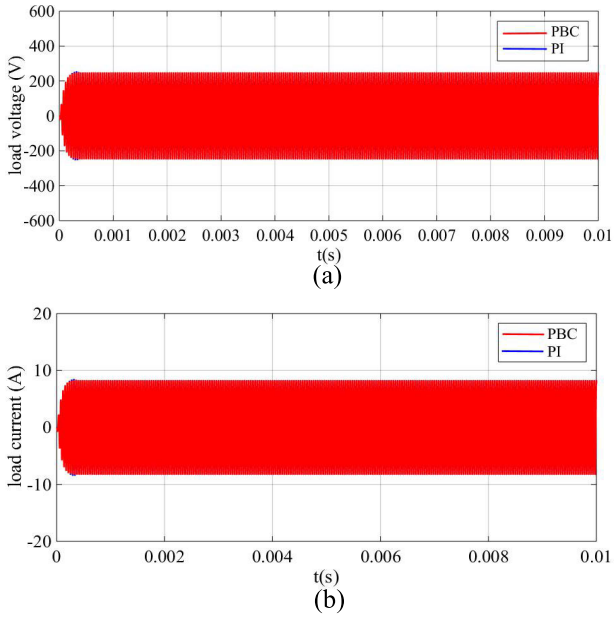

FIGURE 13. Simulation waveform of the load. (a) The voltage waveform of the load; (b) The current waveform of the Load.

TABLE 5. The THD of the load voltage and current.

Control method	THD% of load voltage	THD% of load current
PBC	0.06	0.08
PI	0.15	0.17

Fig. 14(c) shows the power factor response curve. The ICPT system is controlled by the unity power factor in the process of supplying power to the loads, the reference value of the output reactive power is set as zero. Fig.14 (b) shows a comparison of the reactive power response performance between the PI controller and the PBC. The PBC has a smaller overshoot, which makes the reactive power response curve track the reactive power reference in a short time. It effectively overcomes the problems of excessive overshoot and long response time caused by many parameters of the PI controller. Therefore, compared with the PI controllers, the PBC does not need to adjust many parameters, thereby efficiently reducing the design complexity of the control system. In the process of a step change of active power, the reactive power is almost unaffected, thereby proving that the PBC can effectively realize independent control between the active power and reactive power.

To maintain the stable coil transmission efficiency η of the system under internal parameter changes and external interference, the reference value of the transmission efficiency η can be set to a constant value. Fig.14 (d) shows a comparison of transmission efficiency η response performance between the PI controller and the PBC. From the response curve, the PBC makes the transmission efficiency response always maintain a stable value. Instead, the PI controller has a large overshoot, which makes the transmission efficiency of the system intermittently fluctuate greatly. Generally, by using the PBC, the active and reactive power P, Q and transmission efficiency η will be less disturbed than the PI controller, and the THD of voltage and current will also be reduced.

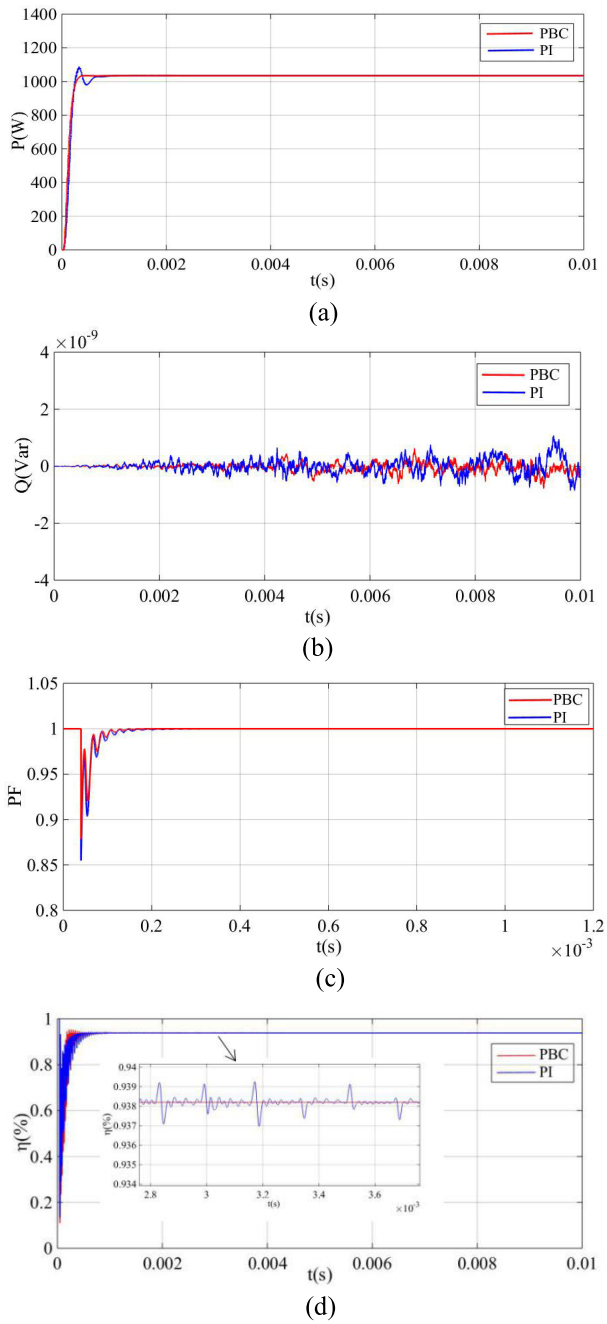

FIGURE 14. Simulation waveform. (a) Waveform of the active power P; (b) Waveform of the reactive power Q; (c) Power factor response curve; (d) Transmission efficiency η.

VI. CONCLUSIONS

This paper analyzed the performance of the movable multi-load ICPT system operating under the influence of mutual inductance parameters and load randomness. A PCHD model of the ICPT system was established, and the passivity-based controller for the ICPT was designed under such conditions. In the current stage, the accuracy of the research results was

verified by simulation experiments. The conclusions of this paper are as follows.

1) The PBC with a precise mathematical model and a few adjustable parameters have low control complexity, strong robustness, and satisfactory performance in both steady-state and dynamic states. The controller effectively overcomes the drawbacks of the PI controller and improves the overall performance of the ICPT system.
2) The ICPT system with the PBC can provide a quick response to suppress the fluctuation of transmission power and efficiency caused by mutual inductance parameters and load randomness, and also effective in THD reduction.

For hardware limitations, some tests are not carried out, future work will involve further testing of the overall performance of the proposed ICPT system.

REFERENCES

[1] J. T. Boys, G. A. Covic, and A. W. Green, "Stability and control of inductively coupled power transfer systems," *IEE Proc.-Electr. Power Appl.*, vol. 147, no. 1, pp. 37–43, Jan. 2000.
[2] Y. Li, R. Mai, M. Yang, and Z. He, "Cascaded multi-level inverter based IPT systems for high power applications," *J. Power Electron.*, vol. 15, no. 6, pp. 1508–1516, Nov. 2015.
[3] Y.-L. Li, Y. Sun, and X. Dai, "Robust control for an uncertain LCL resonant ICPT system using LMI method," *Control Eng. Pract.*, vol. 21, no. 1, pp. 31–41, Jan. 2013.
[4] X. Dai, K. Yu, and Y. Sun, "Study on H_∞ control method for CLC resonant inductive power transfer system," *Proc. CSEE*, vol. 30, no. 30, pp. 47–54, Sep. 2010.
[5] X. Dai, Y. Zou, and Y. Sun, "Uncertainty modeling and robust control for LCL resonant inductive power transfer system," *J. Power Electron.*, vol. 13, no. 5, pp. 814–828, Sep. 2013.
[6] Y.-L. Li, Y. Sun, and X. Dai, "μ-synthesis for frequency uncertainty of the ICPT system," *IEEE Trans. Ind. Electron.*, vol. 60, no. 1, pp. 291–300, Jan. 2013.
[7] C. Xia, W. Wang, G. Chen, X. Wu, S. Zhou, and Y. Sun, "Robust control for the relay ICPT system under external disturbance and parametric uncertainty," *IEEE Trans. Control Syst. Technol.*, vol. 25, no. 6, pp. 2168–2175, Nov. 2017.
[8] C. Xia, W. Wang, S. Ren, X. Wu, and Y. Sun, "Robust control for inductively coupled power transfer systems with coil misalignment," *IEEE Trans. Power Electron.*, vol. 33, no. 9, pp. 8110–8122, Sep. 2018.
[9] H. Hao, G. A. Covic, and J. T. Boys, "An approximate dynamic model of LCL-*T*-based inductive power transfer power supplies," *IEEE Trans. Power Electron.*, vol. 29, no. 10, pp. 5554–5567, Oct. 2014.
[10] R. V. Meshram, M. Bhagwat, S. Khade, S. R. Wagh, A. M. Stankovic, and N. M. Singh, "Port-controlled phasor Hamiltonian modeling and IDA-PBC control of solid-state transformer," *IEEE Trans. Control Syst. Technol.*, vol. 27, no. 1, pp. 161–174, Jan. 2019.
[11] Y. Gupta, K. Chatterjee, and S. Doolla, "Controller design, analysis and testing of a three-phase VSI using IDA-PBC approach," *IET Power Electron.*, vol. 13, no. 2, pp. 346–355, Feb. 2020.
[12] M. N. Uddin, Z. Zhai, and I. K. Amin, "Port controlled hamilton with dissipation-based speed control of IPMSM drive," *IEEE Trans. Power Electron.*, vol. 35, no. 2, pp. 1742–1752, Feb. 2020.
[13] J. Huang, H. Wang, and C. Wang, "Passivity-based control of a doubly fed induction generator system under unbalanced grid voltage conditions," *Energies*, vol. 10, no. 8, p. 1139, Aug. 2017.
[14] B. Zhang, J. Wang, and F. Zhao, "The PCHD model and control of TNPC PV grid-connected inverter," *Proc. CSEE*, vol. 34, pp. 204–210, Nov. 2014.
[15] J. Wang, X. Mu, and Q.-K. Li, "Study of passivity-based decoupling control of T-NPC PV grid-connected inverter," *IEEE Trans. Ind. Electron.*, vol. 64, no. 9, pp. 7542–7551, Sep. 2017.
[16] H. Komurcugil, "Improved passivity-based control method and its robustness analysis for single-phase uninterruptible power supply inverters," *IET Power Electron.*, vol. 8, no. 8, pp. 1558–1570, Aug. 2015.
[17] M. Bottcher, J. Dannehl, and F. W. Fuchs, "Interconnection and damping assignment passivity-based current control of grid-connected PWM converter with LCL-filter," in *Proc. 14th Int. Power Electron. Motion Control Conf. (EPE/PEMC)*, Sep. 2010, pp. T3-20–T3-26.
[18] X. Wang, F. Blaabjerg, and P. C. Loh, "Passivity-based stability analysis and damping injection for multiparalleled VSCs with LCL filters," *IEEE Trans. Power Electron.*, vol. 32, no. 11, pp. 8922–8935, Nov. 2017.
[19] X. Mu, J. Wang, W. Wu, and F. Blaabjerg, "A modified multifrequency passivity-based control for shunt active power filter with Model-Parameter-Adaptive capability," *IEEE Trans. Ind. Electron.*, vol. 65, no. 1, pp. 760–769, Jan. 2018.
[20] Y. Gui, W. Kim, and C. C. Chung, "Passivity-based control with nonlinear damping for type 2 STATCOM systems," *IEEE Trans. Power Syst.*, vol. 31, no. 4, pp. 2824–2833, Jul. 2016.
[21] T.-S. Lee, "Lagrangian modeling and passivity-based control of three-phase AC/DC voltage-source converters," *IEEE Trans. Ind. Electron.*, vol. 51, no. 4, pp. 892–902, Aug. 2004.
[22] M. Mehrasa, M. E. Adabi, E. Pouresmaeil, and J. Adabi, "Passivity-based control technique for integration of DG resources into the power grid," *Int. J. Elect. Power Energy Syst.*, vol. 58, pp. 281–290, Jun. 2014.
[23] Y. Lei, X. Lin, and Y. Zhu, "Passivity-based control strategy for SMES under an unbalanced voltage condition," *IEEE Access*, vol. 6, pp. 28768–28776, 2018.
[24] J. A. Acosta, R. Ortega, A. Astolfi, and A. D. Mahindrakar, "Interconnection and damping assignment passivity-based control of mechanical systems with underactuation degree one," *IEEE Trans. Autom. Control*, vol. 50, no. 12, pp. 1936–1955, Dec. 2005.
[25] W. Gil-González, O. D. Montoya, and A. Garces, "Direct power control of electrical energy storage systems: A passivity-based PI approach," *Electr. Power Syst. Res.*, vol. 175, Oct. 2019, Art. no. 105885.
[26] J. Hua, H.-Z. Wang, Y. Zhao, and A.-L. Zou, "LCL resonant compensation of movable ICPT systems with a multi-load," *J. Power Electron.*, vol. 15, no. 6, pp. 1654–1663, Nov. 2015.
[27] Y. Wang, Y. Hu, and G. Chen, "A novel modulation scheme and a DC-link voltage balancing control strategy for T-type H-bridge cascaded multilevel converters," *J. Power Electron.*, vol. 16, no. 6, pp. 2099–2108, Nov. 2016.
[28] M. Calais, L. J. Borle, and V. G. Agelidis, "Analysis of multicarrier PWM methods for a single-phase five level inverter," in *Proc. IEEE PESC*, Jun. 2001, pp. 1351–1356.
[29] M. S. Reza, M. Ciobotaru, and V. G. Agelidis, "Accurate estimation of single-phase grid voltage parameters under distorted conditions," *IEEE Trans. Power Del.*, vol. 29, no. 3, pp. 1138–1146, Jun. 2014.
[30] X. Fan, L. Guan, C. Xia, J. He, X. Li, and S. Xu, "PCHD-based passivity control of VSC-HVDC connected large wind farm," *Energy Power Eng.*, vol. 5, no. 4, pp. 1209–1214, 2013.
[31] B. Yang, W. Li, Y. Zhao, and X. He, "Design and analysis of a grid-connected photovoltaic power system," *IEEE Trans. Power Electron.*, vol. 25, no. 4, pp. 992–1000, Apr. 2010.
[32] Y. Q. Meng, Y. Li, and J. Liu, "Design of passivity-based control system with integral stability link in flexible HVDC transmission system," *Autom. Electr. Power Syst.*, vol. 38, no. 23, pp. 77–84, Dec. 2014.
[33] P. Wang, J. Wang, and Z. Xu, "Passivity-based control of three phase voltage source PWM rectifiers based on PCHD model," in *Proc. 11th IEEE Int. Conf. Elect. Mach. Syst. (ICEMS)*, Beijing, China, Oct. 2008, pp. 1126–1130.
[34] Y. Liu, J. Xu, Z. Shuai, Y. Li, G. Cui, S. Hu, and B. Xie, "Passivity-based decoupling control strategy of single-phase LCL-type VSRs for harmonics suppression in railway power systems," *Int. J. Electr. Power Energy Syst.*, vol. 117, May 2020, Art. no. 105698.
[35] Y. Jiang, C. Qin, X. Xing, X. Li, and C. Zhang, "A hybrid passivity-based control strategy for three-level T-type inverter in LVRT operation," *IEEE J. Emerg. Sel. Topics Power Electron.*, early access, Jul. 15, 2019, doi: 10.1109/JESTPE.2019.2928571.
[36] W. Rui, S. Qiuye, M. Dazhong, and H. Xuguang, "Line impedance cooperative stability region identification method for grid-tied inverters under weak grids," *IEEE Trans. Smart Grid*, early access, Jan. 29, 2020, doi: 10.1109/TSG.2020.2970174.
[37] D. del Puerto-Flores, J. M. A. Scherpen, M. Liserre, M. M. J. de Vries, M. J. Kransse, and V. G. Monopoli, "Passivity-based control by series/parallel damping of single-phase PWM voltage source converter," *IEEE Trans. Control Syst. Technol.*, vol. 22, no. 4, pp. 1310–1322, Jul. 2014.
[38] R. Wang, Q. Sun, P. Zhang, Y. Gui, D. Qin, and P. Wang, "Reduced-order transfer function model of the droop-controlled inverter via Jordan continued-fraction expansion," *IEEE Trans. Energy Convers.*, early access, Mar. 12, 2020, doi: 10.1109/TEC.2020.2980033.

XIN LI was born in Kunming, Yunnan, in 1978. He received the Ph.D. degree in traffic information engineering and control from Lanzhou Jiaotong University, in 2013. He has been involved in teaching and research of electrified transportation and energy fusion technology.

XIANG LI was born in Lanzhou, Gansu, in 1994. He received the B.S. degree from the School of New Energy and Power Engineering, Lanzhou Jiaotong University, Lanzhou, Gansu, China, in 2018, where he is currently pursuing the M.S. degree with the School of Automation and Electrical Engineering. His research interest is in wireless power transmission systems.